TOWARDS LARGE EDDY SIMULATION OF LNG POOL FIRES

Z.B. Chen, S. Dembele, J.X. Wen[1] and V.H.Y. Tam
Centre for Fire and Explosion Studies, Faculty of Engineering, Kingston University, Friars Avenue, London, SW15 3DW, UK
[1]Correspondence: j.wen@kingston.ac.uk

This paper reports on the results from the first phase of a PhD research programme to develop efficient large eddy simulation (LES) approach for liquefied natural gas (LNG) fires. Soot formation is included using an empirical relationship which Raj (2007a–c) derived from the smoke production measurements in crude oil fires by Notarianni et al. (1993). The effect of soot in obscuring the thermal radiation from different parts of the fire is hence included in the LES simulation while the spectral characteristics of LNG fires are considered via a 6-band model. Predictions are carried out for a 14 m diameter LNG pool fire, which was part of the China Lake test series (Raj et al., 1979). A comparative analysis in terms of temperature, soot density and radiant intensity between the predictions, experimental data and previous analysis is undertaken. The possible implication of the current use of a soot correlation derived from a different and sootier fuel is discussed along with possible directions for improvement. Although more scenarios need to be investigated for a better evaluation of the present approach to predict radiant heat fluxes, the preliminary results are encouraging, demonstrating the potential of the technique to predict thermal radiation hazards from large LNG pool fires.

KEYWORDS: LNG pool fire; FDS; soot model; radiant intensity

INTRODUCTION

In an expert panel convened recently in the US to rank the need for research on LNG, large fire phenomena resulted from LNG spill was ranked as having the highest priority. As a result, the US Department of Energy has provided multi-million dollar funding for Sandia Laboratory to carry out a series of large LNG fires tests (Blanchat et al., 2007).

Previous studies on LNG fires have primarily been based on experimental tests leading to semi-empirical models (Raj et al., 1979; Raj, 2005, 2007a–c; Cleaver et al., 2007; Hanlin, 2006; Koopman and Ermak, 2007). While numerical simulations based on field modelling techniques are now routinely used for the simulations of many fire scenarios (e.g. offshore production facilities, commercial buildings, etc.), limited attempts have been reported on LNG or large scale pool fires. A major barrier is the lack of robust soot model. The close coupling of soot and radiation in such large fires is key in any rigorous modelling approach. This is particularly so for LNG which has complex radiation characteristics.

Raj et al. (1979) and Considine (1984) considered LNG fire emissions to come from both gaseous band emissions and continuous emission from luminous soot and provided approaches to calculate the grey body emissivity as a function of fire size. Although progress has since been made in various fronts, a robust soot model is still lacking for fire simulations in general and it is even so for large LNG fires. For many years, the fire community has relied upon soot models derived for premixed combustion in the engine environment, e.g. various versions of the two equation soot models, which may or may not be valid for fires where combustion occurs through a sequence of local mixing which has dominant effect on the formation of unburned soot and its subsequent oxidation (De Ris et al., 2000 and De Ris, 2009).

An approach relating soot formation to laminar smoke height (the flame height immediately prior to the flame emitting smoke) of both single component and multiple fuels seems promising (Lautenberger et al., 2005). Recently this model has also been extended to account for soot formation and oxidation in fires using a flamelet approach (Chatterjee et al., 2009). Although the lack of comprehensive measurement of smoke points for methane flames in quiescent environment may hinder the application of this approach to LNG fires, the recent work of Berry and Roberts (2006) who measured equal velocity smoke point height for methane, can potentially lead to quiescent condition measurement either by these authors or others. It is clear that this approach still requires further verification by experiments and a robust combustion model to provide the strain rate that is required for the flamelet computation. However, it is worth testing this approach published data on large LNG.

There are no experimental data for soot yield in either small or large methane (or LNG) fires. Neither is there any data for the smoke extinction coefficient for soot formed in methane fires. From the observation of the Montoir 35 m LNG fire tests, Nedelka et al. (1989) commented that large diameter LNG fires seem to produce significant amounts of smoke similar to those observed in the burning of other liquid fuels such as propane, butane, gasoline, kerosene, crude oil and JP4 of higher hydrocarbon content (Raj, 2007b). In the core of large fires, there is insufficient oxygen to burn the carbon produced by the pyrolysis of fuel vapour, leading to lower overall heat release and temperature. In addition, the recirculation of burnt gases by toroidal vortices in all large fires could reduce the

effective mixing of fuel and air in the core and further reduce the combustion efficiency there. However, this is not sufficient to conclude that soot production in large LNG fires is quantitatively the same as in other hydrocarbon fires.

Raj (2007b) derived a correlation for smoke yield from the smoke production measurements in crude oil fires by Notarianni et al. (1993). In the absence of LNG data, Raj used this to calculate the variation of the emissive power with distance for the 35 m Montoir fire tests. The comparison with data suggested that the above correlation may be appropriate for large LNG fires as well. Although only new experimental results can verify whether this assumption is valid, as a first step of the current PhD programme and in anticipation of the expected released of the recently completed Sandia LNG fire tests, it is thought useful to see whether a combined use of this correlation and a spectral band radiation model can predict radiation hazards from LNG fires with reasonable accuracy.

Moreover, in order to calculate thermal radiation hazards distances around large scale LNG pool fires, semi-empirical models such as the solid flame model (SFM) are widely used. SFM assume the fire as a circular cylinder (vertical or tilted) of diameter equal to the base diameter of the fire and axial length representing the visible plume of the fire. To calculate radiation heat flux at a given location with SFM, the Surface Emissive Power (SEP) derived from experiments and the view factor should both be known (Raj, 2007b). This is one of the limitations of SFM. In the conventional SFM, the smoke obscuration that tends to reduce radiation, is not accounted for. A variant of SFM for large hydrocarbon pool fires is the "two-zone" model of McGrattan et al., 2000, which assumes that the lower luminous region is the only radiating surface and upper fire plume is obscured by opaque smoke. A "three-zone" semi-empirical approach that accounts for the variation of the SEP with height was proposed by Raj, 2007b. In spite of these improvements, SFM and its variants are semi-empirical approaches and cannot properly account for the dynamics of large LNG fires.

Large scale tests conducted with different liquid fuels have shown that the burning characteristics and physical behaviour of pool fire changes as the size of the fire increases (Raj et al., 1979). It is hence erroneous to extrapolate results especially thermal radiation emissions from small scale experiments to large size fires. Raj (2007b) commented that the current generation of models used by the scientific community and regulatory agencies, for predicting hazard zones surrounding postulated large LNG pool fires suffer from this problem. The result is the prediction of overly conservative and alarmingly large hazard zones, which, needless to say, cause public alarm. CFD approach, employed in the present study could provide a good alternative for such large LNG fires.

MATHEMATICAL MODELS

HYDRODYNAMIC AND COMBUSTION MODEL

The LES based Fire Dynamics Simulator (FDS) developed by the National Institute of Standards and Technology (NIST) in the USA is adopted as the basic numerical tool. FDS solves the Navier-Stokes equations suitable for low speed, thermally-driven flow using explicit predictor-corrector scheme with second order accuracy in space and time (McGrattan and Forney, 2004). The Smagorinski model is used for sub-grid level turbulence with the default model constant of 0.2 and the default value of 0.5 is used for both the Prandtl and Schmidt numbers.

For combustion, the default mixture fraction model is used. The corresponding species concentration are obtained based on the following reaction equation (Eq. (1)) by referring to the look-up table, which is constructed in advance and contains concentrations of fuel, oxygen and other products as function of the mixture fraction (McGrattan and Forney, 2004):

$$C_xH_yO_z + \upsilon_{O_2}O_2 \rightarrow \upsilon_{CO_2}CO_2 + \upsilon_{H_2O}H_2O + \upsilon_{CO}CO + \upsilon_{Soot}Soot \quad (1)$$

where υ_{O_2}, υ_{CO_2}, υ_{H_2O}, υ_{CO} and υ_{Soot} are specified as the ideal stoichiometric coefficients for O_2, CO_2, H_2O, CO and soot, respectively.

SOOT MODEL

Following Raj (2007b), soot concentration Cs (kg/m^3) is related to the burning efficiency of the fuel (β), the heat of combustion of the fuel (ΔH_c), the stoichiometric air to fuel mass ratio (r) and the soot mass yield per unit mass of fuel burned (Y) by the formula:

$$C_s = \frac{\rho_0 Y}{1 + (r/\beta) + (\Delta H_c/c_0 T_0)}, \quad (2)$$

where ρ_0, c_0 and T_0 are respectively the air density, specific heat and temperature. In the present context, β is the combustion efficiency factor (fraction of the mass of air entrained at any location that burns with its stoichiometric equivalent mass of fuel) and is assumed as a constant throughout the combustion zone.

As mentioned earlier, there are no experimental data for soot yield in large methane (or LNG) fires. Notarianni et al. (1993) measured the smoke production in crude oil fires of diameters from 0.085 m to 17.2 m and found that smoke yield (mass in % of burnt fuel that is emitted as smoke) increases as the diameter of the fire increases. Raj (2007b) correlated the data for the smoke yield, Y, versus fire diameter of these crude oil fires tests with the following equation:

$$Y = 9.412 + 2.758 \times \log_{10}(D), \quad (3)$$

where D is the fire base diameter. Raj (2007b) then combined this with the model he proposed for the variation of the emissive power with distance through fire plume and applied it to the 35 m Montoir LNG fire tests and the China lake tests with r set to 17.17 and β to 0.06. The favourable comparison of the predicted and measured

mean SEP over the visible fire plume height (as further discussed below) showed that the above correlation may be appropriate for large methane fires as well. While it is appreciated that more experimental results will be required to verify this assumption, it is thought useful to see if combined with the LES code, reasonable predictions can be made about the radiation hazards in LNG fires.

As this correlation was derived from experimental measurements, we can also assume that soot oxidation in the fire is implicitly accounted for and hence no specific modelling consideration is given to this aspect.

RADIATION MODEL

For radiation calculation, FDS uses the Finite Volume Method (FVM) to solve the Radiative Transfer Equation (RTE). For optically thick flames (large soot amount), a grey gas approach could be used with reasonable accuracy. In optically thin flames where the amount of soot is small, radiation by gaseous species (H_2O and CO_2) needs to be accounted for by a non-grey model. This is achieved in the present study by dividing the radiation spectrum into a number of bands (typically 6), and a separate RTE is derived for each band. An analysis of the spectral data of the China Lake 14 m diameter LNG pool fire experiments by Raj (2007c) has shown that the flame is optically thin, therefore the non-grey FVM option in FDS is employed for the present simulations.

EXPERIMENTS CONSIDERED

Numerical simulations were conducted for Test 12 with 14 m diameter in the China Lake test series which involved spilling LNG on water in a 50 m × 50 m × 1 m pond. The test was the only one in the series conducted in zero wind condition and the only test for which both the wide angle radiometer (WAR) data and narrow angle radiometer (NAR) data were analyzed to obtain SEP. As mentioned in many previous studies and by Raj (2007a), NAR SEP (only available for the 15 m) is based on a very narrow portion of the flame and as such does not represent the overall flame SEP. Only WAR data could provide overall SEP which is more reliable.

The volume of LNG spilled was 5.7 m^3 with spill rate of 0.07 m^3/s. The release lasted around 81 s while the intense burning was recorded as lasting 75 s. The fire base diameter was 14 m and the visible flame length was measured as 44.0 m ± 6.3 m. The average LNG burning rate was measured as 4.94×10^{-4} m/s, corresponding to the mass loss rate per area of 0.22 kg/m^2s. The WAR was directed at 1.5 m above the fire base and 30 m from the fire centre while two NAR were also set at the location 30 m from the pool centre but with height of 4.6 m and 6.2 m above the fire base. Measurements indicated that the atmospheric absorption corrected SEP by WAR was 220 ± 47 kW/m^2 and spot SEP by NAR was 224 ± 13 k W/m^2.

NUMERICAL SIMULATION DETAILS

A domain with size of 100 × 100 × 100 m is employed in the simulations of the China Lake experiment. A circular pool with diameter of 14 m is located in the middle. The boundaries of the domain except the ground are defined as 'opening', which meant that fire smoke and fresh air could exchange at these boundaries.

The domain is divided into several mesh blocks to facilitate parallel computing on multi-processor computers. Finer grid resolutions are used for the flame region and its immediate surrounding 30 × 30 × 60 m than elsewhere in the calculation domain (see Table 1). For simplicity, this region will be referred to as the "fire region" hereafter. All the simulated cases are summarized in Table 1. The 'False' mode of synchronization indicates that meshes are updated separately and the time steps are different for each mesh. The benefit is saving in computing time. In contrast, the 'True' mode means times are forced to be the same for different mesh blocks. Although it might increase computing time, the connection among the different mesh blocks is tighter than that the 'False' mode.

Since the China Lake Tests were conducted on water, heat release rate would be steady. In each simulation, steady heat release rate of 11,000 kW/m^2 was set on the upper surface of the fire base. This was achieved by multiplying the mass loss rate per area and the heat of combustion (50 MJ/kg). The simulations were found to reach

Table 1. Simulation cases

	Grid resolution (m)			
	Region near fire	Other region	Operation system	Synchronization
Case 1	0.45 × 0.45 × 0.45	1.0 × 1.0 × 1.0	Windows PC (64 bit)	False
Case 2	0.36 × 0.36 × 0.36	1.0 × 1.0 × 1.0	Windows PC (64 bit)	False
Case 3	0.33 × 0.33 × 0.33	1.0 × 1.0 × 1.0	Windows PC (64 bit)	False
Case 4	0.25 × 0.25 × 0.25	1.0 × 1.0 × 1.0	Linux cluster (64 bit)	False
Case 5	0.25 × 0.25 × 0.25	0.5 × 0.5 × 0.5	Linux cluster (64 bit)	False
Case 6	0.25 × 0.25 × 0.25	0.5 × 0.5 × 0.5	Linux cluster (64 bit)	True
Case 7	0.20 × 0.20 × 0.20	0.5 × 0.5 × 0.5	Linux cluster (64 bit)	True

quasi-steady state in about 15 s physical time and but were continued for another 15 s to allow the fire to be fully developed.

RESULTS AND DISCUSSIONS

EFFECT OF GRID RESOLUTION AND SYNCHRONIZATION

It is well known that grid resolution can influence LES predictions, and this is especially true for the FDS code. McGrattan and Forney (2004) provided criteria to estimate spatial resolution in terms of the characteristic diameter of a plume. However if this criteria is applied to such large fires, it would give much coarser grid resolution than what is actually required. We have hence conducted grid sensitivity study with a range of grid resolutions from 0.2 m to 0.45 m as listed in Table 1 and used the average centreline temperature to check their effect on the predictions. It can be seen in Figure 1a that all predictions follow the same trend, i.e. the centreline temperature firstly increases with the increase of height and start to decrease after reaching the maximum value on some location with height varying from 20 m to 25 m. However, there are considerable differences in the actual values of the predicted temperatures except near the fire base. Specifically, refining the grid resolution in the fire zone from 0.45 m to 0.33 m has resulted in major changes in the predicted temperatures especially in the region from 20 m to 25 m above the pool surface. There are relatively smaller changes in the predicted temperatures when the grid resolution is refined from 0.33 m to 0.25 m (Figure 1a). For Cases 4 and 5, the predicted centreline temperatures are almost the same as expected since the special resolution in the fire region is kept constant. For Cases 5 and 6, grid synchronization has shown considerable effect on the predictions. It is therefore recommended that for multi-block calculations on the cluster, setting of synchronization should be 'True' in FDS to ensure close coupling of different mesh blocks while there is no need to use this for the simulation on a single processor. For Cases 6 and 7, the predictions are very close apart from the persistent flame zone, where the temperatures are actually lower than the outer region due to lack of oxygen in the core region of the large fire. All of the predictions presented and discussed below are based on Case 6.

TEMPERATURE AND VELOCITY

In Figure 1b, the predicted centreline temperature variations (case 6) are compared with McCaffrey's (1975) data and correlations. While McCaffrey's tests for fire sizes of between 14 to 60 kW more or less collapsed onto a single curve after non-dimensionalized against the total heat output, significant differences exist between the current predictions for the 14 m diameter LNG fire with 1210 MW heat output and these small fire data, especially in the lower part. The smaller laboratory scale fires were found in previous experiments and numerical predictions including that of our own (Liu and Wen, 2002) to have almost constant temperatures but this is obviously not the case for large fires, where there is generally a relatively large fuel rich core inside the flame due to lack of oxygen to support combustion. This finding is consistent with results from previous field experiments conducted with different liquid fuels which suggested that the burning characteristics and physical behaviour of pool fires change as the size (diameter) of the fires increases. With increasing fire size, flame temperature usually increases because of decreasing thermal radiation loss from the fire. This may be the main reason why the predicted centreline temperatures for the intermittent and plume regions are higher than laboratory fires. The comparison also shows that extrapolation of the results (especially thermal radiation emissions) from

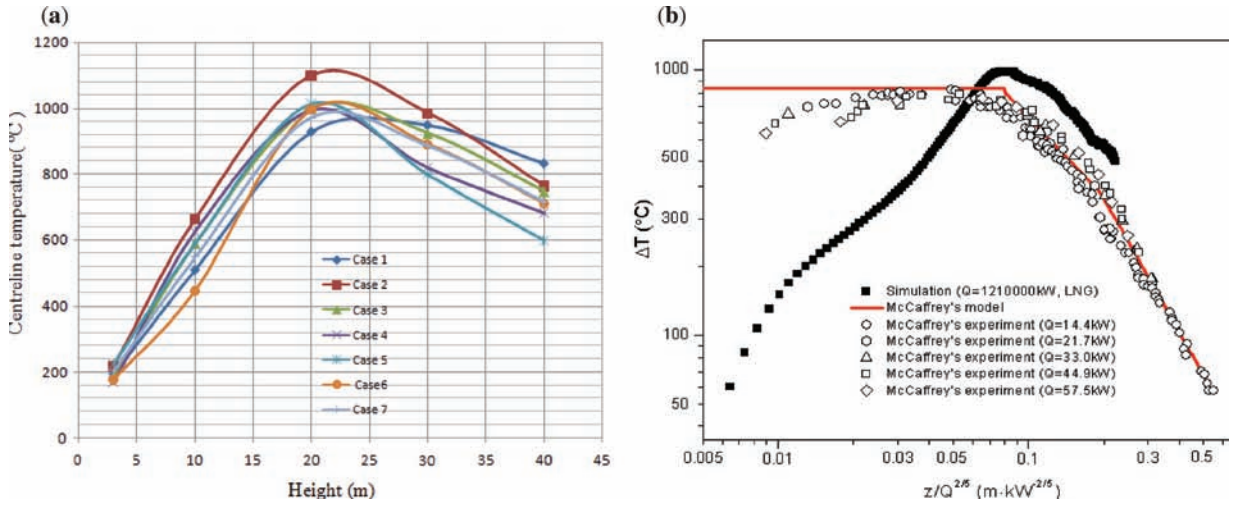

Figure 1. (a) Predicted centreline temperature variations with height for different cases, (b) comparison of the predicted centreline temperature in Case 6 with McCaffrey's (1975) data and correlation

small-scale experiments for predicting the characteristics of large size fires occurring in postulated accidental liquid fuel release scenarios (from terminal storage tanks, ships, barges and other large volume transports) is prone to significant errors.

The bottom region of a pool fire is generally referred to as the "persistent flame zone", where most chemical reactions take place and the combustion of the fuel vapour is considered to be very efficient (only in the outer layers of vapours for large fires) and the fire goes through laminar to turbulent transition driven by buoyancy in the near field. The intense chemical reactions and air entrainment in this region is of dominant effect on flame establishment. While the work of McCaffrey and others have led to well established correlations for centreline temperature for the entire fire plume, the lack of detailed measurements in large fires have not made it possible to derive temperature correlations. The present predictions indicate that the slope of the centreline temperature in the intermittent and plume region in large fires may be very similar to that of small fires but the persistent flame region follows a completely different trend. It may be possible to develop new correlations for large fires by conducting numerical tests with different diameter fires and fuels; and on this basis to verify the predictions with at least some carefully selected tests where there are near field temperature measurements. It should also be possible to conduct validated numerical experiments to establish the limiting size (diameter) of fires where McCaffrey's correlation ceases to be valid and new correlation needs to be developed to assist risk assessment where detailed CFD simulations cannot be conducted for economical or operational reasons.

The predicted instantaneous temperature contours for the period when heat release rate reached quasi steady state are shown in Figure 2a. The puffing of the fire is evidenced by the fluctuations of the flame height. According to Pagni's (1990) formula for pool fire puffing frequency, $f^2 = \frac{2.3}{D}$, where D is the fire base diameter. The predicted puff frequency of a 14 m diameter fire is about 0.40 Hz corresponding to a puff cycle of approximately 2.5 s. The six instantaneous plots here can be considered as representation of the variations in a puff cycle. The shaded contours of the mean temperature obtained by averaging between physical time of $20 \sim 30$ s is shown in Figure 2b. It can be seen that the predicted temperatures inside the flame is $1000 \sim 1400$ K, which is consistent with the range of 1300 K–1500 K quoted by Raj (2007b). The predicted flame height is also in the same range as measurement which was 44 m $\pm$ 6.3 m.

The predicted mean radial temperatures at different heights are plotted in Figure 3a, b. The double humped shape of temperature distributions along the radial direction is found when the height is less than 20 m, which means that average temperatures in the core region (radial distance 50 m) are lower than the outer region. This points to the existence of a fuel rich core as oxygen in the entrained air is mostly consumed before it reaches the core of the persistent flame zone. Up to 2 m high in the core region, there is almost no combustion at all. With increase of height, more entrained air reaches the core due to increasing turbulence level and the large scale vortices as shown in Figure 4a, b, resulting in enhanced fuel air mixing and more complete combustion and consequently higher temperatures in the core region. But further up, more

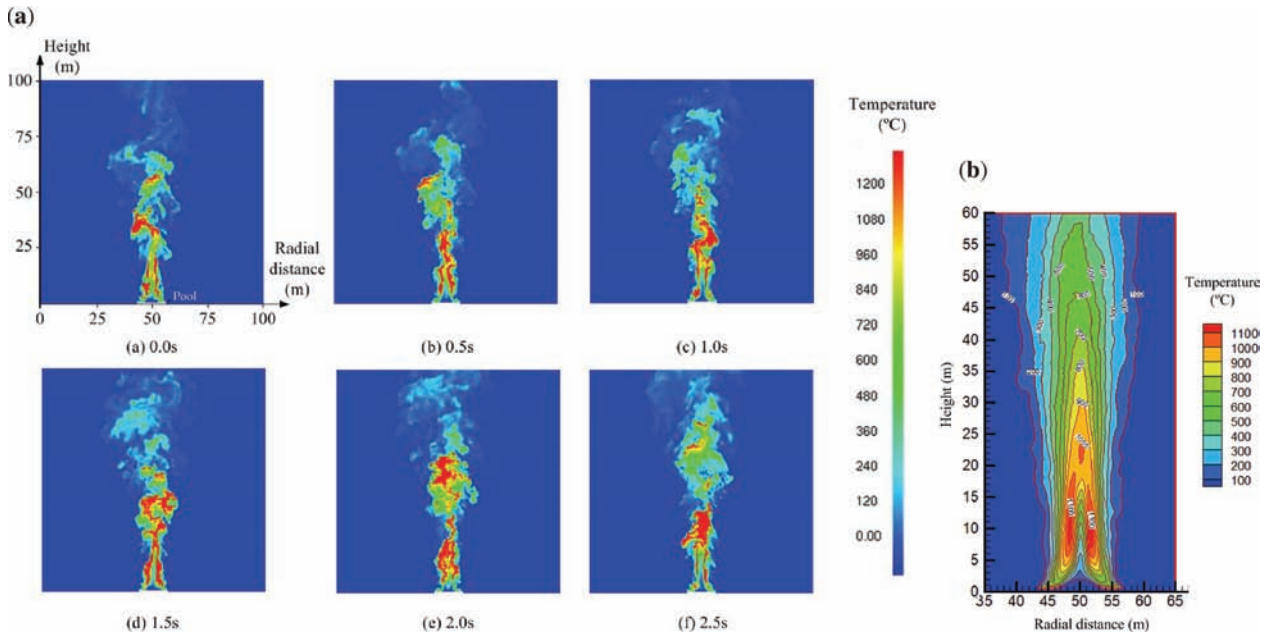

Figure 2. (a) Instantaneous temperature contours in a puff cycle, (b) mean temperature

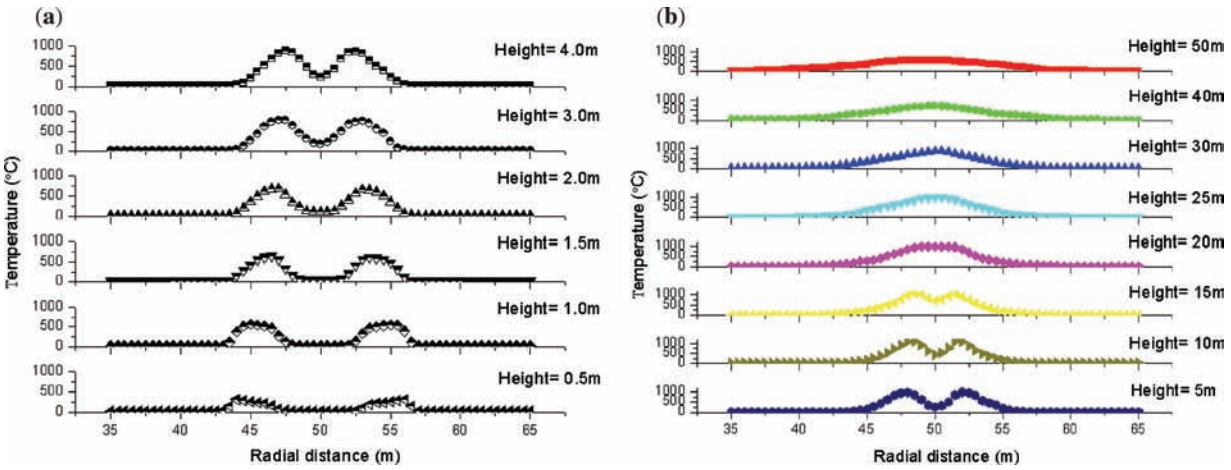

Figure 3. (a, b) Radial temperature distributions at different heights

entrained air is brought into the fire plume and mix with the combustion products resulting in temperature decrease in the intermittent and plume regions. The formation and shedding of large scale toroidal vortices can also be seen in Figure 4a, b.

SOOT DENSITY

Figure 5 describes the instantaneous soot density distribution for the periods as the instantaneous temperature results presented in Figure 2a. It can be seen that in the upper part, the soot density is relatively larger than that in the flame area. This is consistent with previous experimental findings. As explained by De Ris (2009), soot progressively forms in the rising fire and gradually accumulates as its oxidation rate is lower than that of fuel vapour.

Soot density distribution along the radial direction at different heights is plotted in Figure 6. For the region between 5 m to 15 m high, soot concentration near the centreline (about 800 mg/m^3) is greater than that in the outer regions (about 500 mg/m^3). Further up, the soot density profile gradually expands in the radial direction as more unburnt soot is driven up and outwards by the rising and expanding hot gases.

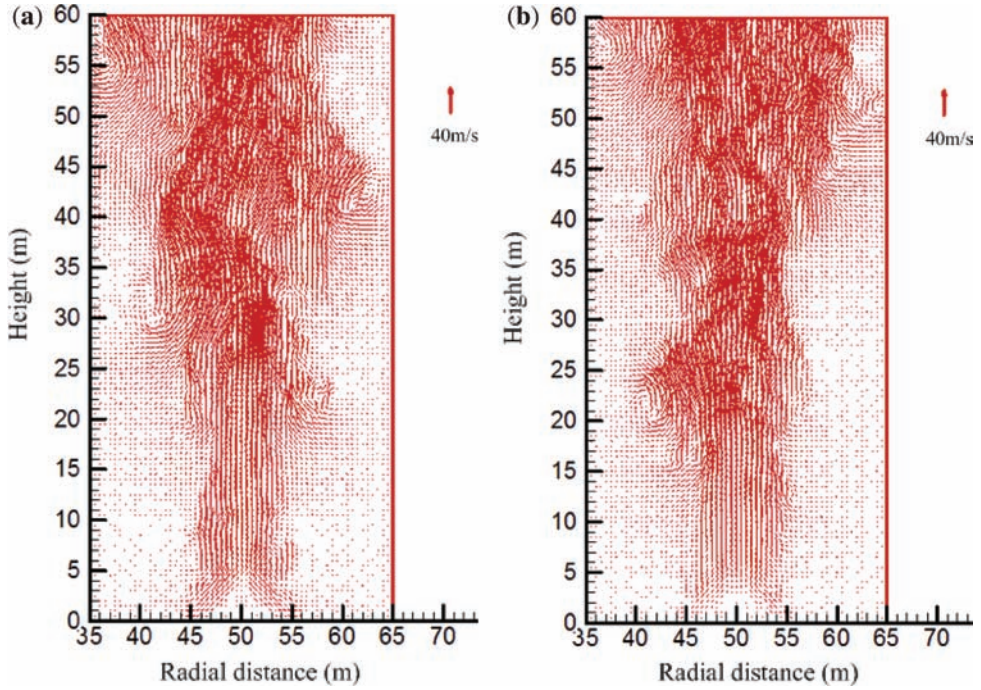

Figure 4. (a, b) Two instantaneous velocity fields at the centre plane of the fire plume captured

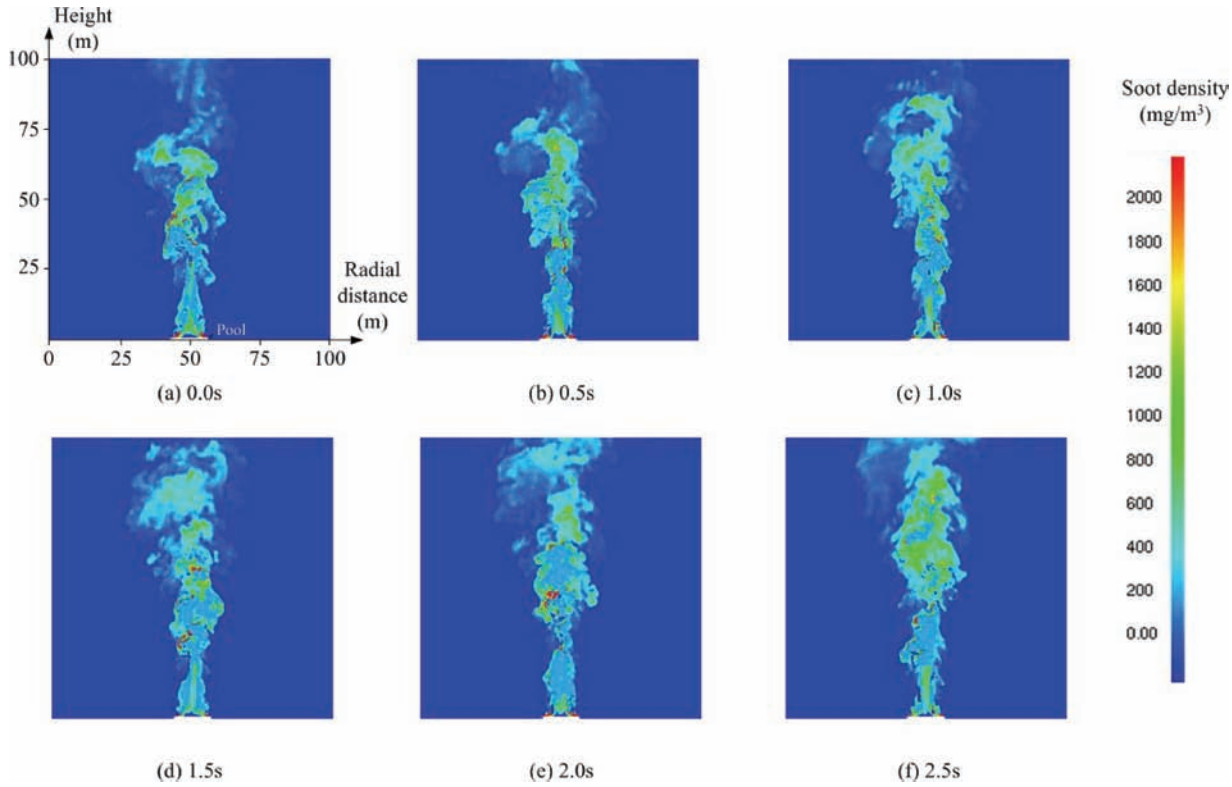

Figure 5. Instantaneous soot density contours

RADIANT HEAT FLUX

The predicted instantaneous radiation heat flux distributions are presented in Figure 7a while the mean value is plotted in Figure 7b. Radiation heat flux was not measured within the flame envelope in the experiment. The WAR was located 30 m from pool centre. Therefore there was no data for direct comparison of radiant heat flux within the flame. However the SEP of the flame calculated from the WAR experimental data using the measured visible flame length of $44.0\,\text{m} \pm 6.3\,\text{m}$ is $220 \pm 47\,\text{kW/m}^2$ (Raj, 2007a). This means that in the SFM approach, a cylinder of 44 m high and 14 m diameter approximating the actual flame would radiate an average heat flux of $220\,\text{kW/m}^2$ from its surface. In Figure 7b, radiant heat fluxes predicted within the flame are in the range of $0 \sim 1000\,\text{kW/m}^2$. Heat fluxes on the outer surface of the flame over the visible length are approximately in the range of 200–$300\,\text{kW/m}^2$. This is quantitatively consistent with the SEP inferred from the experimental measurements.

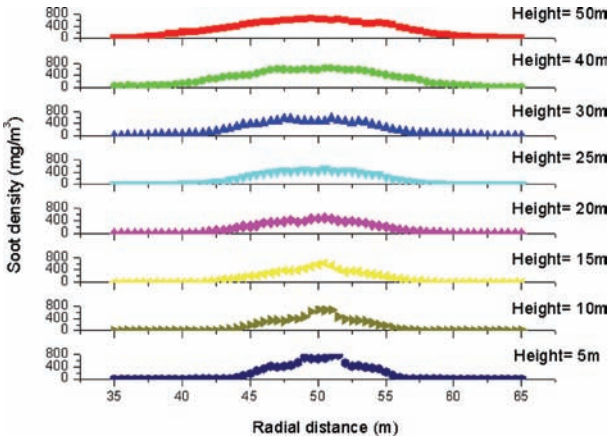

Figure 6. Radial soot density distributions at different heights

In hazards analysis both instantaneous and mean radiation fluxes are of significance. Comparing Figures 7a and 7b, it is worth noting that there are pockets within the flame where the radiant heat fluxes are higher than the maximum average values.

As heat flux was measured by the WAR located 30 m from pool centre, the predictions at WAR location are analysed. The image for the very small region in the core (just above the pool surface corresponding to the WAR location (30 m from the pool centre, 1.5 m high from ground level)) at time 1.5 s in Figure 7a is typically redrawn in Figure 8 in order to understand the radiant hazards in surroundings. In Figure 8, the black border line corresponds approximately to the WAR location where the predicted transient radiative heat flux is about $7.8\,\text{kW/m}^2$. For the steady period of the fire, the predicted radiant heat flux varied between

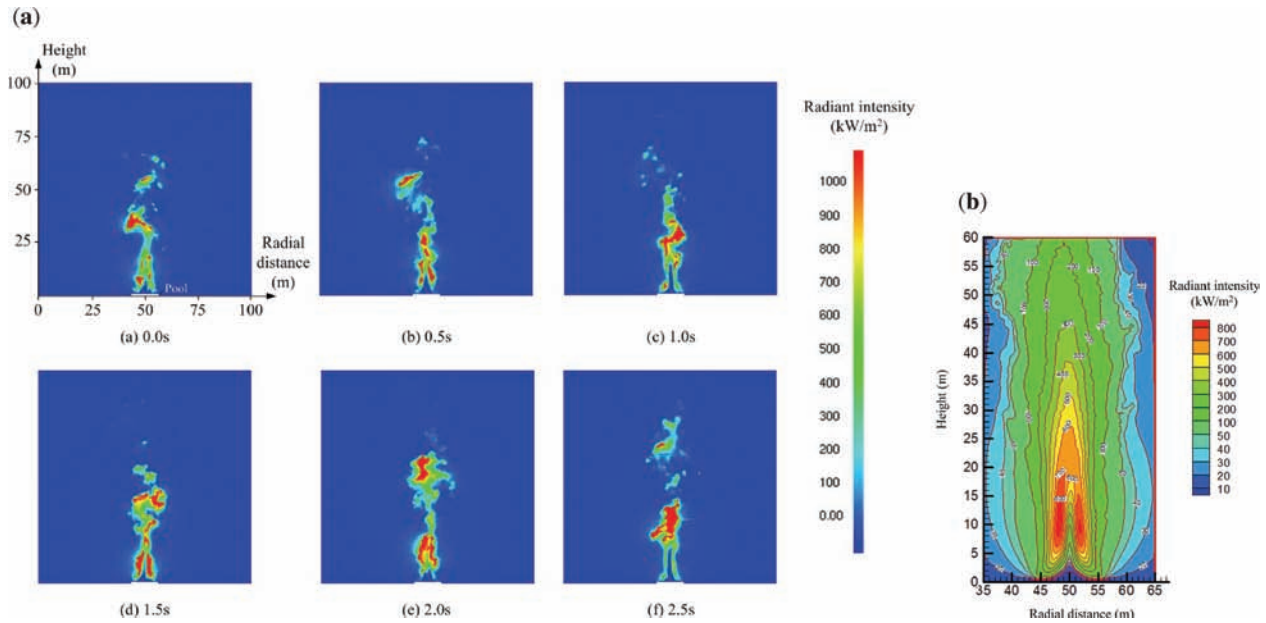

Figure 7. (a) Instantaneous radiant intensity contour (across pool centreline), (b) mean radiant intensity

4 kW/m^2 and 12 kW/m^2 at the WAR location (average predicted value around 8 kW/m^2). From experiments the heat flux measured by the WAR was about 18 kW/m^2 (Raj, 1979). The predicted average value of 8 kW/m^2 is lower than the measurement. Raj (1979) developed a semi-empirical model to predict radiant heat flux at locations outside the flame. The radiative heat flux predicted by Raj's model at the WAR location was 8.6 kW/m^2, which is similar to the present prediction. The higher radiant heat flux measured by the WAR could in part be explained by its lower location near the flame base and other experimental errors as discussed by Raj (1979).

Figure 9 describes the radiant heat flux variation with height at different radial distances. Radiant heat fluxex have not been measured within the flame envelope in the China Lake experiments. The WAR and NAR data gave a cylinder of 44.0 m height and 14 m diameter in SFM. The corresponding radial location of the flame theoretical surface 57 m in Figure 9 (radial distance 50 m is the pool centre). The radiant heat fluxes are consistently larger for radial location closer to the pool centre as expected near the combustion zones. For all radial locations there is a gradual decay of radiant heat flux in the upper region of

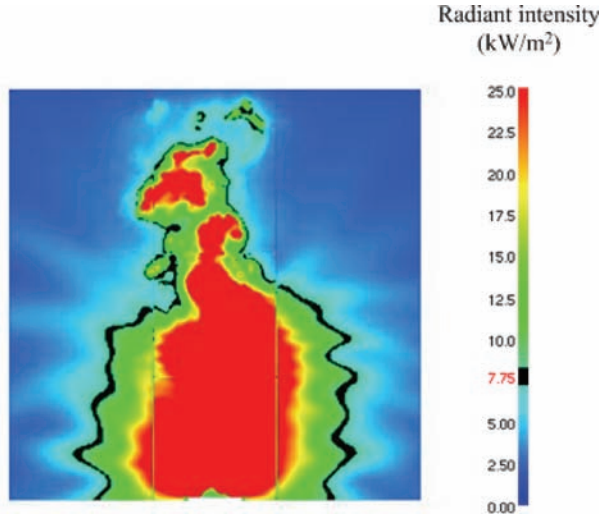

Figure 8. Radiant intensity distribution (N.B. This is a blown up plot of a very small region 30 m from pool centre and 1.5 m high, i.e. part of the blue region in the core of Figure 7a)

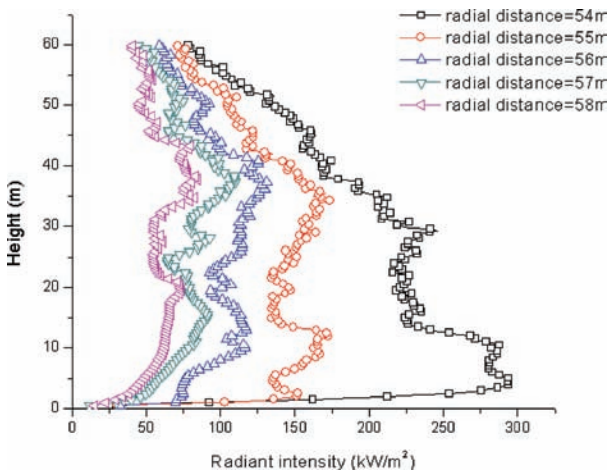

Figure 9. Variation of radiation intensity at different locations

plume consistent with SEP decrease in the intermittent region (Raj, 2007b).

As mentioned earlier, NAR measured directly the spot emissive power on the flame. Therefore, comparison with NAR data can be conducted if the theoretical flame interface in the region near the fire base is achieved. The actual experimental visible flame interface is bound to fluctuate due to the turbulent nature of the pool fire, thus the radial distance varied from 54 m (4 m from pool centre) to 58 m to account for the uncertainties in the location of the visible flame interface. When the height varies from 3 m to 10 m, it is found that with decrease of radial distance from 58 m to 54 m the difference of radiant intensity between two adjacent curves are more important. The radiant intensity at the location with radial distance of 54 m is nearly two times greater than that with radial distance of 55 m. It is highly possible that the local zone ("spot") at radial distance of 54 m and height ranging from 3 m to 10 m is on the visible flame interface (surface). The average "spot" radiant heat flux from the predictions is at the 270 kW/m^2 point in Figure 9. This value could be compared with the NAR "spot" SEP of 224 $\pm$ 13 kW/m^2 obtained from the large scale tests (Raj, 2007a). There is reasonable agreement between the two sets of data. For a rigorous comparison with the WAR data based on the total visible length (and not local height), the total visible flame interface from predictions should be identified and the heat flux averaged over the total flame length, which is a cumbersome task which we have not undertaken. Although more scenarios need to be investigated for a better evaluation of the present approach to predict radiant heat fluxes, the preliminary results are encouraging, demonstrating the potential of the technique to predict thermal radiation hazards from large LNG pool fires.

CONCLUSIONS

A large eddy simulation approach has been developed to simulate LNG pool fires incorporating empirically derived correlation for soot production and finite volume method for radiation with the wide band model. Numerical predictions were carried out for the 14 m diameter LNG fire test in the China Lake Tests series. The predicted instantaneous temperature, soot and radiant intensity profiles across the pool centreline show that there is fuel rich core in the persistent flame region. This is thought to be due to insufficient oxygen there for complete combustion. The predicted maximum flame temperature is in line with previous experimental findings.

Comparison of the predicted centreline temperature with McCaffrey's (1975) data and correlations for laboratory scale pool fires have further proved that the burning characteristics and physical behaviour of pool fires changes as the size of the fire increases and it is erroneous to extrapolate results especially thermal radiation emissions from small scale experiments for predicting the characteristics of large size fires. The present study has also shown that it may be possible to develop new correlations for large fires by conducting numerical tests with validated numerical models for different diameter fires and fuels. It should also be possible through this process to establish the limiting size (diameter) of fires where McCaffrey's correlation ceases to be valid and new correlation needs to be developed to assist risk assessment where detailed CFD simulations cannot be conducted for economical or operational reasons.

The average soot density in the flame is around 500 mg/m^3, which is in the same order as the predicted value (332.8 mg/m^3) of Raj (2007b). The predicted radiant heat flux at the WAR location in the field test ranges from 4 kW/m^2 to 12 kW/m^2 giving an average predicted value of around 8 kW/m^2, while radiometer gives about 18 kW/m^2 and the value predicted by Raj et al. (1979) using his model is about 8.6 kW/m^2. As explained by Raj et al. (1979), the relatively higher radiant heat flux measured by the WAR was erroneous due to its lower location near the flame base and other experimental errors. The present prediction is hence in line with Raj's analysis of the measured data.

It was also found that there are pockets within the flame where the radiant heat fluxes are higher than the maximum average values. This raises caution about risk analysis based on the predictions of the mean radiant intensity using semi-empirical models.

ACKNOWLEDGEMENTS

The author gratefully acknowledges the Nation Funding Scholarship sponsored by China Scholarship Council (CSC) and Overseas Research Students Awards Scheme (ORSAS) funded by Higher Education Funding Council for England (HEFCE).

REFERENCES

Berry, T. and Roberts, W., 2006, Measurement of smoke point in velocity-matched co-flow laminar diffusion flames with pure fuels at elevated pressures, *Combustion and Flame*, 145: 571–578.

Blanchat, T., Luketa-Hanlin, A., Hightower, M. and Tieszen, S., 2007, Briefing to NARUC Staff Subcommittee on Gas.

Chatterjee, P., et al. 2009, Soot and Radiation Models, *FM Global Open Source CFD Fire Modeling Workshop*, Boston, USA.

Cleaver, P., Johnson, M. and Ho, B., 2007, A summary of some experimental data on LNG safety, *Journal of Hazardous Materials*, 140: 429–438.

Considine, M., 1984, Thermal Radiation Hazard Ranges from Large Hydrocarbon Pool Fires, *Report No. SRD R297, Safety & Reliability Directorate*, UK Atomic Energy Authority, UK.

De Ris, J., 2009, Smoke mantle of large pool fires (Private communication).

De Ris, J., Wu, P. and Heskestad, G., 2000, Radiation Fire Modelling, *Symp (Int) on Combustion*, 28.

Hanlin, A., 2006, A review of large-scale LNG spills: Experiments and modelling, *Journal of Hazardous Materials*, A132: 119–140.

Koopman, R. and Ermak, D., 2007, Lessons learned from LNG safety research, *Journal of Hazardous Materials*, 140: 412–428.

Lautenberger, C., De Ris, J., Dembsey, N., Barnett J. and Baum H., 2005, A simplified model for soot formation and oxidation in CFD simulation of non-premixed hydrocarbon flames, *Fire Safety Journal*, 40(2): 141–176.

Liu, F. and Wen, J., 2002, The effect of different turbulence models on the CFD simulation of buoyant diffusion flames, *Fire Safety Journal*, 37: 125–151.

McCaffrey, B., 1975, Purely buoyant diffusion flames: some experimental results, *NBSIR-79/1910, National Bureau of Standards, USA*.

McGrattan, K., Baum, H.R. and Hamins, A., 2000, Thermal Radiation from Large Pool Fires, NISTIR 6546, National Institute of Standards and Technology, USA.

McGrattan, K. and Forney, G., 2004, Fire dynamics simulator Version 4), Technical Reference Guide, *NIST Special Publication 1018*, National Institute of Standards and Technology, USA.

Nedelka, D., Moorhouse, J. and Tucker, R.F., 1989, The Montoir 35 m Diameter LNG Pool Fire Experiments, LNG9, Nice, France.

Notarianni, K., Evans, D., Walton, W., Madrzykowski, D. and Lawson J., 1993, C.A. Franks (Ed.), Smoke Production from Large Oil Pool Fires, Interflam 1993, Oxford/London, England.

Pagni, P., 1990, Pool vortex shedding frequencies, *Applied Mechanics Review*, 43: 153–170.

Raj, P., 2005, Large LNG fire thermal radiation-modeling issues and hazard criteria revisited, *Process Safety Progress*, 24: 192–202.

Raj, P., 2007a, LNG fires: A review of experimental results, models and hazard prediction challenges, *Journal of Hazardous Materials*, 140: 444–464.

Raj, P., 2007b, Large hydrocarbon fuel pool fires: Physical characteristics and thermal emission variations with height, *Journal of Hazardous Materials*, 140: 280–292.

Raj, P., 2007c, LNG fire spectral data and calculation of emissive power, *Journal of Hazardous Materials*, 142: 720–729.

Raj, P., Moussa, A. and Aravamudan, K., 1979, Experiments involving pool and vapour fires from spills of LNG on water, *NTIS AD-A077073, USCG Report GD-D-55-79*, Washington, DC.